ADVANCED OPTICAL MATERIALS
www.advopticalmat.de

Controllable Propulsion by Light: Steering a Solar Sail via Tunable Radiation Pressure

*Dakang Ma, Joseph Murray, and Jeremy N. Munday**

Photons carry momentum, which can be transferred to an object upon reflection or absorption. The resulting force from light is rather weak but can have macroscopic consequences, e.g., sunlight imparts momentum on dust particles causing a comet's tail to be directed away from the sun, as first suggested by German astronomer Kepler in 1619.[1,2] Maxwell later predicted that light is capable of imparting momentum on an object based on his wave-theory of electromagnetism in 1873,[3] which was shown experimentally by Lebedev in 1901[4] and Nichols and Hull in 1903.[5] Due to the development of opto-micro-mechanical devices, there is a renewed interest in the measurement of radiation pressure on micromechanical structures in both vacuum and ambient environment.[6,7]

The concept of radiation pressure for space propulsion has a long history in both popular culture and as a next generation space technology.[8,9] Most space missions are limited by the amount of chemical propellant carried on board; however, as an alternative, solar sails use solar radiation pressure as propulsion and offer an opportunity for propellant-free space travel, enabling long-term and long-distance missions that are impossible with traditional methods. Although solar sail propulsion alleviates the need to carry chemical fuel, attitude control, and steering are still performed using traditional methods involving reaction wheels and propellant ejection. A propellant-less attitude control mechanism would reduce weight and cost while improving performance and lifetime for solar sail missions. One way to achieve attitude control is to incorporate materials whose optical properties can be altered electronically, so that radiation pressure on different parts of a solar sail can be controlled individually and actively during operation. The IKAROS (Interplanetary Kite-craft Accelerated by Radiation Of the Sun) mission from the Japan Aerospace eXploration Agency successfully demonstrated the use of a reflective control device (RCD) to achieve limited attitude control of a spinning-type solar sail.[10] The ideal material for attitude control should have significant momentum transfer difference between on and off states over a broad range of the solar spectrum.

For the past few decades, liquid crystal devices have been used in numerous light control applications.[11,12] Among those, polymer dispersed liquid crystal (PDLC) films stand out due to their ability to be switched from an opaque to a transparent state with the applied external electric field without the need for polarizers. Since its discovery,[13] researchers have extensively explored the potential applications of PDLCs in the areas of flat panel displays,[14] smart windows,[15,16] microlens,[17] etcetera. PDLC films consist of liquid crystal microdroplets dispersed in a polymer matrix. The liquid crystal droplets are optically birefringent with ordinary refractive index n_o and extraordinary refractive index n_e, while the polymer is an optically isotropic material with refractive index n_p. In the absence of an applied electric field (off state), the optical axes of individual bipolar droplets align randomly, resulting in spatial variations of refractive indices across the film. Liquid crystal microdroplets whose refractive indices differ from polymer matrix strongly scatter light and the PDLC film appears hazy. When enough voltage is applied across the film (on state), the liquid crystal molecules, which have positive dielectric anisotropy, align their optical axes with the electric field so that light incident normal to the film experiences a refractive index n_o in the liquid crystal droplets. By choosing the appropriate liquid crystal and polymer so that n_o and n_p are equal, the film becomes highly transparent as a result of reduced light scattering in the on state.[18] Unlike traditional liquid crystal displays, which need polarizers and waste half of the light in the bright state, PDLCs do not require polarizers, offering much higher optical/energy efficiency. PDLCs also have significant optical contrast between on and off states over a broad range of the solar spectrum and the ability to be fabricated on a flexible substrate, both of which make it an ideal material for solar sail attitude control. Further, researchers have recently shown that polyimide-based PDLC films have potential for aerospace applications due to radiation tolerance.[19–21]

In this Communication, we present a steerable solar sail concept based on a PDLC that switches between transparent and scattering states, enabling attitude control without mechanically moving parts or chemical propellant. Devices are fabricated and characterized (transmission, reflection, absorption and scattering) over the visible and near infrared range of solar spectrum (400–1100 nm) and are found to outperform previous designs by more than a factor of four in terms of overall weighted momentum switchablility between on and off states. Devices require no power in the diffusely reflective state and dissipate <0.5 mW cm^{-2} while in the on state, showing great potential as a low-power switching mechanism for solar sail attitude control.

Figure 1 shows an exemplary design of a solar sail incorporating PDLC devices. The main part of the solar sail is coated with highly reflective aluminum to provide maximum thrust from solar radiation pressure. PDLC devices are attached to the sail edges to maximize the torque generated from the radiation

D. Ma, Dr. J. Murray, Prof. J. N. Munday
Department of Electrical and Computer Engineering
University of Maryland
College Park, MD 20742, USA
E-mail: jnmunday@umd.edu
D. Ma, Dr. J. Murray, Prof. J. N. Munday
Institute for Research in Electronics
and Applied Physics
University of Maryland
College Park, MD 20742, USA

DOI: 10.1002/adom.201600668

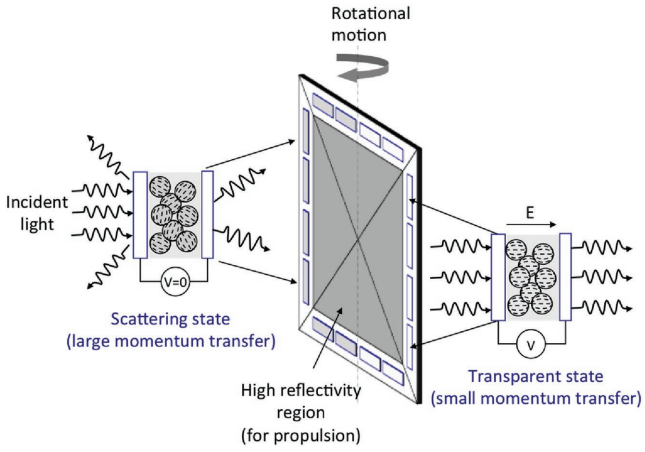

Figure 1. Schematic showing propellantless altitude control of a solar sail using PDLC devices. The optical properties of PDLC devices are controlled individually, which results in spatial-variation of the radiation pressure across the solar sail.

pressure difference between on and off states. In Figure 1, PDLC devices on the left are in the off state and scatter into both the forward and backward directions, resulting in a larger radiation pressure than those on the right, which are in the transmissive on state.

To demonstrate the potential momentum switchablity of PDLCs, a 33 µm thick PDLC cell made from E7 nematic liquid crystal and Norland Optical Adhesive (NOA65) was prepared by the phase separation method (see the Experimental Section). This thickness provides a good balance between high scattering in the off state and low turn-on voltage.

A common method to determine the light scattering properties of a device is to measure its direct transmission with collection optics of a well-defined *f*-number (*f*/12 is commonly used, equivalent to a collection angle of 4.8°).[22] A supercontinuum tunable laser (Fianium WhiteLase SC400UV) is used as the light source, and a homemade high-voltage driving circuit provides the square-wave AC voltages needed to turn the PDLC cell from opaque to transparent. The direct transmission is determined as a function of both wavelength and applied voltage as the device switches between the transmissive on state and the opaque off state (**Figure 2**a).

For a typical PDLC device, the direct transmission can be varied from 0% to >80% upon switching. As the input wavelength increases from 400 to 750 nm, the direct transmission increases monotonically with wavelength. Both off state and on state transmission as well as turn-on voltage is greater at longer wavelengths, because the scattering cross sections at long wavelengths are smaller than those at short wavelengths under the same degree of droplet director alignment (same electric field) based on the anomalous diffraction model of scattering.[23,24] Despite some wavelength dependence, the significant optical contrast provided by the switchable scattering of PDLC is broadband in nature (Figure 2c).

In order to calculate the momentum transferred to the PDLC device, the angular distribution of light scattering of the PDLC cell under normal incidence is measured to determine the fraction of light scattered to different angles and their corresponding contribution to the total momentum transfer (**Figure 3**a). The angular distribution of the scattering under increasing applied voltage is shown in Figure 3b. In the off state (zero applied field), the scattering profile is very broad with a small amount of direct transmission (<0.2% at 632.8 nm). The full-width-half-maximum of the diffusive scattering profile (after removing the direct transmission) is about 48°, larger than the 30° predicted by the anomalous diffraction approximation.[12] Multiple scattering causes the intensity to fall off much more slowly with scattering angle because the cell is quite thick compared with the size of liquid crystal microdroplets.[25] As the applied voltage increases, direct transmission and forward scattering gradually increase, and, after reaching the turn-on voltage (V_{90}), scattering reduces dramatically, and the film becomes transparent and is dominated by direct transmission. This sharp change in the scattering profile originates from the strong nonlinear relationship between the applied voltage, degree of droplet director alignment, and scattering cross section.[23]

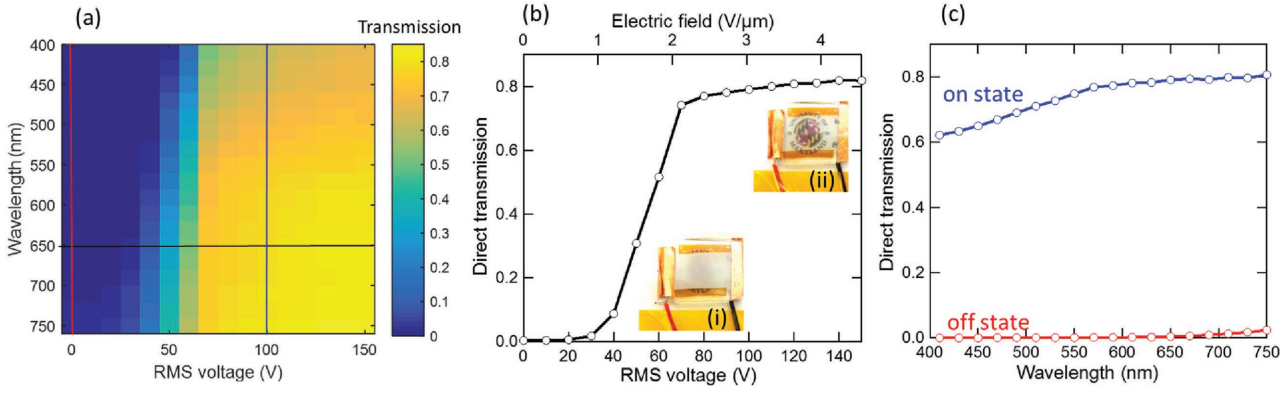

Figure 2. a) The direct transmission as a function of input wavelength and RMS (root mean square) voltage applied to the PDLC cell. b) The direct transmission as a function of RMS voltage at 650 nm, corresponding to the black line in (a). The turn-on voltage V_{90} at this wavelength, where the transmission reaches 90% of the maximum transmission, is 70 V and the corresponding turn-on field is 2.12 V µm^{-1}. Insets: photos of the PDLC cell in the (i) off state and (ii) on state. c) The direct transmission across the visible on state (100 V) and off state (0 V), corresponding to the blue and red lines in (a), respectively.

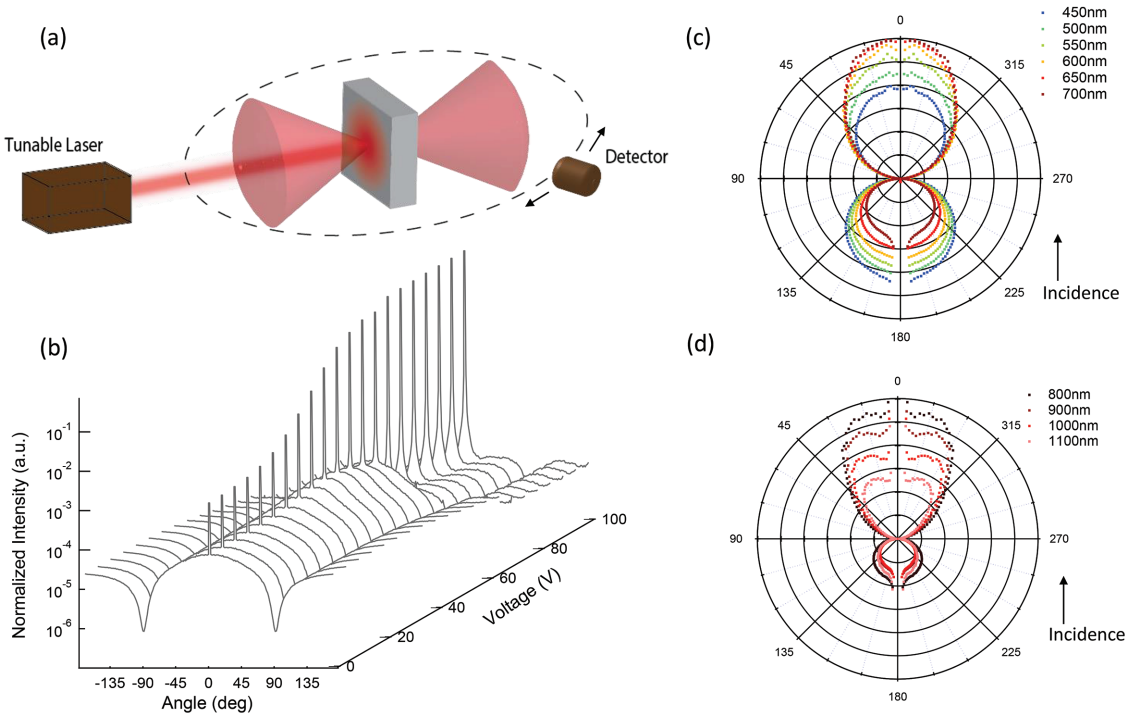

Figure 3. a) Experimental setup for measuring the angular distribution of light scattering for the PDLC cell. Input light is at normal incidence. b) A series of angular distribution measurements using 632.8 nm illumination with increasing voltages applied to the PDLC cell. Each curve shows the optical power measured at different scattering angles normalized to the incident laser power and is mirrored with respect to 0° (incident direction). Scattering distribution of the PDLC in the off state is shown under c) visible and d) infrared illumination.

The angular distributions as a function of wavelength are also measured because it is important for calculating the total momentum transfer under broadband solar illumination (Figure 3c,d). The scattering distribution of the PDLC in the off state shows strong wavelength dependence. As the wavelength increases, a greater fraction of scattered light goes in the forward direction rather than in the backward direction. The Lambertian scattering profile, which was used in a previous work,[10] is a good approximation for scattering at short wavelengths but fails to describe the scattering distribution at longer wavelengths.

The total transmission and absorption of the PDLC in the on and off states are measured in an integrating sphere (see **Figure 4**a and the Experimental Section). The total reflection is calculated from this data as

$$R(\lambda) = 1 - T(\lambda) - A(\lambda) \tag{1}$$

With increasing wavelength, the total transmission increases at first because of reduced scattering and then decreases due to the stronger absorption of the indium tin oxide (ITO) layer at longer wavelengths. The total reflection, on the other hand, decreases (with increasing wavelength) due to the reduced scattering and is finally dominated by specular reflection at the long wavelength end of the spectrum, which is less dependent on the bias across the PDLC film. The ITO layer used in this cell has large absorption in the near infrared because it is optimized for maximum transmission in the visible spectrum while providing good conductivity. We note that the slight difference in the transmission data between Figures 2 and 4 is likely due to sample aging (~1 month) in ambient environment between measurements and slight differences in the measurement techniques. Effects of space environment on the device are beyond the scope of this manuscript but will be considered in future work.

With all the optical properties measured, we can calculate the momentum transferred to the PDLC device under solar illumination. The initial and final momenta of monochromatic photons with momentum magnitude of p_0 are

$$\vec{p}_i = p_0 \hat{s} \tag{2}$$

and

$$\vec{p}_f = p_0 \left[R_s \hat{s} - 2R_s (\hat{n} \cdot \hat{s}) \hat{n} + T_s \hat{s} - R_d C_{Rd} \hat{n} + T_d C_{Td} \hat{n} \right] \tag{3}$$

respectively, where $\hat{n}$ is the surface normal unit vector of the PDLC device, $\hat{s}$ is the unit vector for the initial photon direction, T_s is the direct transmission coefficient (i.e., the fraction of incident photons directly transmitted), R_s is the specular reflection coefficient, T_d is the diffusive transmission coefficient, R_d is the diffusive reflection coefficient, and C_{Rd} and C_{Td} are the diffusive transmission and reflection momentum coefficients. C_{Rd} and C_{Td} represent the average fraction of momenta (absolute value) of diffusively transmitted or diffusively reflected photons, which are calculated from the scattering angular distribution measurement as

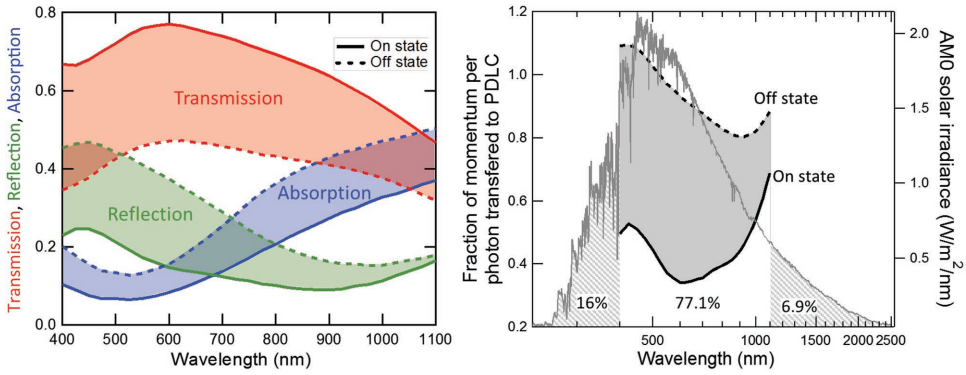

Figure 4. a) Total transmission, absorption, and reflection of the PDLC cell in the on and off states under near normal incidence measured with an integrating sphere. b) Fraction of momentum per photon transferred to PDLC (left axis) in the on and off states at different wavelengths (400–1100 nm) overlaid on the AM0 solar irradiance spectrum (right axis). The measured data covers 77.1% of the total energy (or momentum) of the AM0 solar spectrum.

$$C_{\mathrm{Td}} = \frac{\int_0^{\pi/2} I_{\mathrm{T}}(\theta)\cos\theta\sin\theta\, d\theta}{\int_0^{\pi/2} I_{\mathrm{T}}(\theta)\sin\theta\, d\theta} \tag{4}$$

and

$$C_{\mathrm{Rd}} = \frac{\left|\int_{\pi/2}^{\pi} I_{\mathrm{R}}(\theta)\cos\theta\sin\theta\, d\theta\right|}{\int_{\pi/2}^{\pi} I_{\mathrm{R}}(\theta)\sin\theta\, d\theta} \tag{5}$$

where $I_{\mathrm{T}}(\theta)$ and $I_{\mathrm{R}}(\theta)$ are the measured normalized powers in the scattering profile measurement (Figure 3). The difference in the initial and final momenta is the momentum transferred to the PDLC

$$\vec{p}_{\mathrm{PDLC}} = \vec{p}_{\mathrm{i}} - \vec{p}_{\mathrm{f}} = p_0\left[(1 - T_{\mathrm{s}} - R_{\mathrm{s}})\,\hat{s} + \left(2R_{\mathrm{s}}(\hat{n}\cdot\hat{s}) + R_{\mathrm{d}}C_{\mathrm{Rd}} - T_{\mathrm{d}}C_{\mathrm{Td}}\right)\hat{n}\right] \tag{6}$$

The maximum thrust and greatest switchability occurs when the solar sail is directly facing the sun (normal incidence illumination), which is the case that we will consider. Thus, at normal incidence, $\hat{n}\cdot\hat{s} = 1$, and the above equation reduces to

$$\vec{p}_{\mathrm{PDLC}} = p_0(1 + R_{\mathrm{s}} - T_{\mathrm{s}} + R_{\mathrm{d}}C_{\mathrm{Rd}} - T_{\mathrm{d}}C_{\mathrm{Td}})\,\hat{n} \tag{7}$$

Here we define a wavelength dependent coefficient

$$f_{\mathrm{p}}(\lambda) = 1 + R_{\mathrm{s}}(\lambda) - T_{\mathrm{s}}(\lambda) + R_{\mathrm{d}}(\lambda)C_{\mathrm{Rd}}(\lambda) - T_{\mathrm{d}}(\lambda)C_{\mathrm{Td}}(\lambda) \tag{8}$$

which gives the fraction of momentum per photon transferred to the PDLC, shown in Figure 4b. Because a solar sail would be illuminated by a broadband solar spectrum in space, the weighted average fraction of momentum transferred to the PDLC (in either state) is calculated by

$$f_{\mathrm{avg}} = \frac{\int f_{\mathrm{p}}(\lambda)S(\lambda)\,d\lambda}{\int S(\lambda)\,d\lambda} \tag{9}$$

where $S(\lambda)$ is the AM0 solar irradiance. The change of the fraction of the weighted average momentum transferred to PDLC between the on state and the off state is

$$\Delta f_{\mathrm{avg}} = f_{\mathrm{avg,on}} - f_{\mathrm{avg,off}} \tag{10}$$

$|\Delta f_{\mathrm{avg}}|$ is a primary figure of merit for a switchable solar sail, where larger values of $|\Delta f_{\mathrm{avg}}|$ correspond to greater switchability of the momentum transfer. Over our measurement range, from 400 to 1100 nm, $|\Delta f_{\mathrm{avg}}| \simeq 0.5$.

Compared with the RCD devices on IKAROS that are switched from diffusive scattering in the off state to specular reflection in the on state, our transmissive-type PDLC devices that are switched from diffusive scattering in the off state to direct transmission in the on state provide a larger momentum transfer difference, $|\Delta f_{\mathrm{avg}}|$. Figure of merits of the RCD devices on IKAROS are also calculated based on the data provided in ref. [10], where a Lambertian scattering profile is assumed for all wavelengths rather than measured as in this paper (**Table 1**). Although our measurement range was limited to 400–1000 nm, it covers 77.1% of the energy/momentum available from the AM0 solar spectrum. If the device had no switchability between 300–400 and 1100–2000 nm (which is unlikely), the device would still outperform the RCD devices on IKAROS by nearly a factor of four.

Because the orientations of the liquid crystal droplet directors are determined by the electric field, we further explore the possibility of reducing the turn-on voltage and power consumption of the PDLC device by thinning the PDLC layer. However, a thinner PDLC device potentially has less scattering in the off state and thus will compromise its momentum switchability. To demonstrate the tradeoff, five PDLC cells with different thicknesses but the same PDLC mixture and ITO coated glasses

Table 1. Comparison of figure of merits between our device and IKAROS.

	RCD on IKAROS (300–2000 nm)	Our device (400–1100 nm)
$f_{\mathrm{avg,\,on}}$	1.51	0.43
$f_{\mathrm{avg,\,off}}$	1.40	0.93
$\lvert\Delta f_{\mathrm{avg}}\rvert$	0.11	0.50

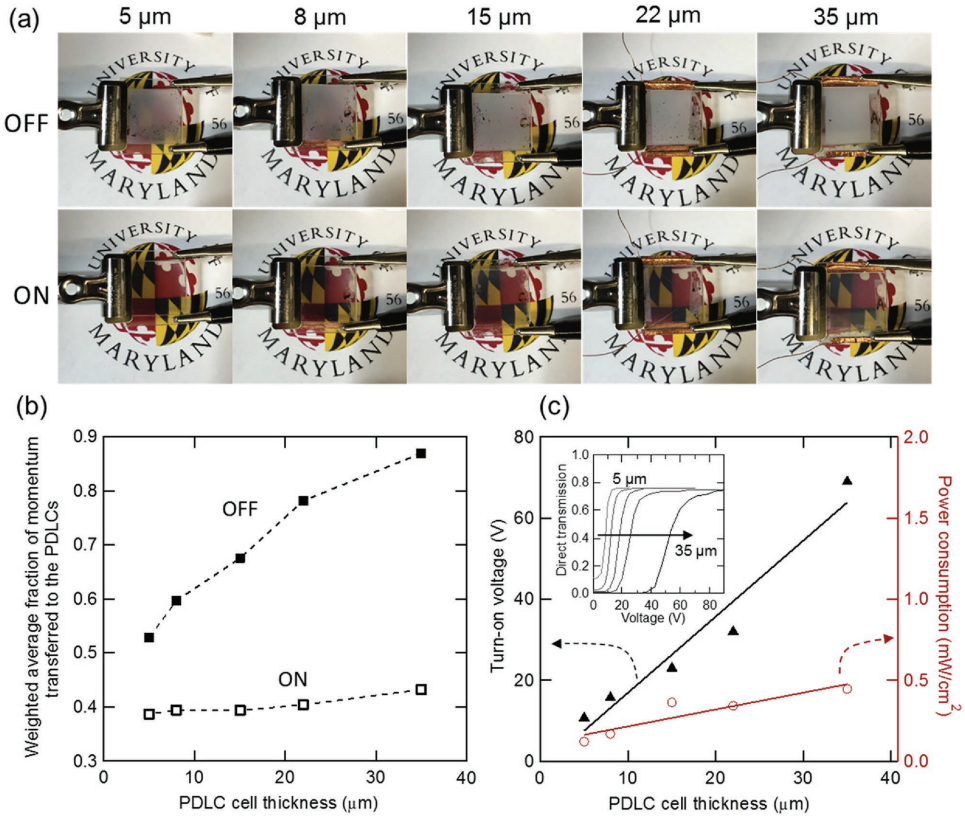

Figure 5. a) Optical images of (1 in × 1 in) devices in the off state (1st row) and the on state (2nd row) of five PDLC cells with increasing thickness from left to right. Cell thickness is measured by optical interferometry.[26] b) Average fraction of momentum transferred to the PDLCs weighed by the AM0 solar spectrum over the measurement range (400–1100 nm) for the five devices. c) Turn-on voltages (left), determined by 90% transmission at 650 nm incident illumination, and power consumption per unit area (right) in the on state as a function of PDLC thickness. The black and red lines are linear fits to the turn-on voltage and power consumption data, respectively. Inset: direct transmission under 650 nm illumination versus applied RMS voltage.

(SPI Supplies) are made and tested. The visual images of these PDLC cells in the on and off states show that the direct transmission in the on states do not change much with thickness but in the off state, thinner cells start to appear more transparent, indicating less scattering and more direct transmission (**Figure 5**a). Optical properties of the five cells are measured following the procedures described above, and the fractions of the weighted average momentum transferred to the PDLCs are calculated (Figure 5b). As expected, momentum transferred to the PDLC in the off state decreases for thinner cells, while the momentum transferred to the PDLC in the on state changes very little. The electrical power consumption of the PDLC cells in the on state is measured (see the Experimental Section) and the turn-on voltages are determined (Figure 5c). They both follow an approximately linear relationship with cell thickness over the voltage range considered in these experiments. Therefore, reducing the PDLC thickness is an effective way to reduce power consumption. Ohmic loss in the ITO and leakage current throughout the device eventually limit the minimum power consumption; however, the reduced switchability for films below a few micrometers will likely restrict how thin these devices can be made for useful solar sail applications.

In summary, we fabricated and characterized a transmissive-type PDLC device for use as an electrically tunable radiation pressure modulator for propellant-less attitude control of a solar sail. The PDLC device provides large, broadband differences in the optical properties between on and off states without the need for polarizers. The measured optical properties (transmission, reflection, absorption, and scattering) are combined to calculate the expected momentum transferred to the device as a function of incident wavelength. The difference in weighted average momentum per photon over the measurement range (400 to 1100 nm, covering 77.1% of the total energy/momentum of the AM0 solar spectrum) between the on and off states can be as large as 0.5, approximately four times higher than previous reflective-type devices. The approach of calculating the momentum transfer of light based on measured data can be applied to other types of scattering materials and devices. Lastly, we showed the impact of PDLC thickness on the optical momentum transfer and electrical power consumption and discussed the trade-off between optical switchablity and power consumption. Thinner cells enable reduced operating voltages and power consumption while thicker cells provide larger momentum difference between the on and off states. The desired thickness of the PDLC device will depend on mission specific requirements but can easily be modified using these techniques. The development of an electrically switchable radiation pressure modulator will enable new functionality for solar sail missions and will expedite the development of long-term and long-distance, propellant-free space flight.

Experimental Section

Device Fabrication: The PDLC consists of liquid crystal mixture E7 (LC Matter Corp.) and photocurable polymer NOA65 (Norland Products) with 1:1 weight ratio. It is filled into an empty cell made with two ITO coated glass slides (Adafruit) with ITO coating facing inward, which is separated by two polyester spacers (McMaster-Carr) on the edges. The PDLC mixture is then cured at room temperature for 1 min with an UV lamp.[22] The two ITO layers are connected to copper wires and the electric field is applied through a custom-built high voltage AC source operating at 100 Hz. E7 has a nematic–isotropic transition temperature at 61 °C and a positive dielectric anisotropy ($\Delta\varepsilon = \varepsilon_{//} - \varepsilon_{\perp}$) at 20 °C, where $\varepsilon_{//}$ and $\varepsilon_{\perp}$ represent the parallel and perpendicular dielectric constants, respectively. The refractive indices of E7 at 20 °C are given as $n_o = 1.5183$; $n_e = 1.7378$ ($\lambda = 632.8$ nm), leading to a birefringence of 0.2195. The melting point is 0 °C.[27]

Transmission and Absorption Measurements: Total transmission and absorption measurements are made using an integrating sphere (Labsphere RTC-060) illuminated by monochromatic light (5 nm bandwidth). Transmission is measured by placing the sample at an open port in the sphere and illuminating through this sample. Absorption measurements are similarly made but with the sample mounted in the center of the sphere. Measurements are made at a near-normal incidence of 13° for absorption measurements and 7° for transmission measurements, where the difference is due to the geometry of the setup. The light intensity in the sphere is detected with a photodiode. A small portion of the incident light beam is diverted to a reference photodiode to account for power variation of the light source. Second order diffuse absorption in the sample (light that is reflected or transmitted by the sample which then scatters and is redirected toward the sample) is accounted for with a diffuse illumination measurement. The signal to noise ratio is enhanced using a chopper and lock-in amplifier configuration (Stanford Research Systems 830).

Scattering Measurement: Scattering distribution measurements are made using a custom goniometer with sample illumination by a Fianium supercontinuum laser at normal incidence. The system rotates a photodiode about the sample and the photocurrent is measured by a Keithley 2400 Source Meter. The height of the photodiode is adjusted to the same height with the input laser to record the optical power along the equator of the scattering profile. The scattering is independent of azimuthal angle.[12]

Electrical Power Consumption: To measure the power consumption of the PDLC device, a load resistor of 1.2 kΩ is connected in series with the PDLC. When the cell is in the on state, the current through the resistor and the voltage across the PDLC device are recorded in the time domain. The product of the current and voltage is then averaged over a period to determine the average power consumption of the PDLC in the on state.

Acknowledgements

The authors acknowledge financial support for this project from a NASA Early Career Faculty Award (No. NNX12AQ50G) and a NASA Smallsat Patnership Award (No. NNX15AW53A). The authors also thank Tiffany Russell Lockett, Andrew Heaton, and Keats Wilkie for many helpful suggestions, comments, and discussions about solar sails.

Received: August 15, 2016
Revised: October 21, 2016
Published online:

[1] U. Leonhardt, *Nature* **2006**, *444*, 823.
[2] J. Kepler, *De Cometis Libelli Tres*, A. Apergerum, Augustae Vindelicorum **1619**.
[3] J. C. Maxwell, *A Treatise on Electricity and Magnetism*, Oxford University, Oxford, UK **1873**.
[4] P. N. Lebedev, *Ann. Phys.* **1901**, *6*, 433.
[5] E. F. Nichols, G. F. Hull, *Phys. Rev. (Ser. I)* **1903**, *17*, 26.
[6] P. R. Wilkinson, G. A. Shaw, J. R. Pratt, *Appl. Phys. Lett.* **2013**, *102*, 184103.
[7] D. Ma, J. L. Garrett, J. N. Munday, *Appl. Phys. Lett.* **2015**, *91107*, 4.
[8] C. R. McInnes, *Solar Sailing: Technology, Dynamics, and Mission Applications*, Springer, New York **2004**.
[9] G. Vulpetti, L. Johnson, G. L. Matloff, *Solar Sails*, Springer, New York **2015**.
[10] R. Funase, Y. Shirasawa, Y. Mimasu, O. Mori, Y. Tsuda, T. Saiki, J. Kawaguchi, *Adv. Space Res.* **2011**, *48*, 1740.
[11] D. Franklin, Y. Chen, A. Vazquez-Guardado, S. Modak, J. Boroumand, D. Xu, S.-T. Wu, D. Chanda, *Nat. Commun.* **2015**, *6*, 7337.
[12] S. T. Wu, D. K. Yang, *Fundamentals of Liquid Crystal Devices*, Wiley, West Sussex, UK **2006**.
[13] J. W. Doane, N. A. Vaz, B.-G. Wu, S. Žumer, *Appl. Phys. Lett.* **1986**, *48*, 269.
[14] J. A. Firehammer, G. P. Crawford, N. M. Lawandy, *Appl. Phys. Lett.* **1998**, *73*, 590.
[15] C. M. Lampert, *Sol. Energy Mater. Sol. Cells* **2003**, *76*, 489.
[16] H. Hosseinzadeh, K. Liew, Y. Han, N. Mohieddin, I. a. Goldthorpe, *Sol. Energy Mater. Sol. Cells* **2015**, *132*, 337.
[17] H. Ren, Y. H. Fan, Y. H. Lin, S. T. Wu, *Opt. Commun.* **2005**, *247*, 101.
[18] D. A. Higgins, *Adv. Mater.* **2000**, *12*, 251.
[19] Y. Gao, P. Song, T. Zhang, W. Yao, H. Ding, J. Xiao, S. Zhu, H. Cao, H. Yang, *RSC Adv.* **2013**, *3*, 23533.
[20] D. Wang, L. Zhang, Y. Xing, H. Gao, K. Wang, Z. Yang, M. Hai, H. Cao, W. He, H. Yang, *Liq. Cryst.* **2015**, *42*, 1689.
[21] T. Zhang, M. Kashima, M. Zhang, F. Liu, P. Song, X. Zhao, C. Zhang, H. Cao, H. Yang, *RSC Adv.* **2012**, *2*, 2144.
[22] P. S. Drzaic, *Liquid Crystal Dispersions*, World Scientific, Singapore **1995**.
[23] J. Kelly, W. Wu, P. Palffy-muhoray, *Mol. Cryst. Liq. Cryst. Sci. Technol., Sect. A* **1992**, *223*, 251.
[24] S. Zŭmer, *Phys. Rev. A* **1988**, *37*, 4006.
[25] J. R. Kelly, W. Wu, *Liq. Cryst.* **1993**, *14*, 1683.
[26] K. H. Yang, *J. Appl. Phys.* **1988**, *64*, 4780.
[27] Y. Derouiche, F. Dubois, R. Douali, C. Legrand, U. Maschke, *Mol. Cryst. Liq. Cryst.* **2011**, *541*, 201.